Methyl rotational tunneling dynamics of *p*-xylene confined in a crystalline zeolite host

Sankar Nair[a)]
*School of Chemical & Biomolecular Engineering, Georgia Institute of Technology, Atlanta,
Georgia 30332-0100*

Robert M. Dimeo and Dan A. Neumann
*NIST Center for Neutron Research, National Institute of Standards and Technology, Gaithersburg,
Maryland 20899-8562*

Anthony J. Horsewill
School of Physics and Astronomy, University of Nottingham, Nottingham NG7 2RD, United Kingdom

Michael Tsapatsis
*Department of Chemical Engineering & Materials Science, University of Minnesota, Minneapolis,
Minnesota 55455-0132*

The methyl rotational tunneling spectrum of *p*-xylene confined in nanoporous zeolite crystals has been measured by inelastic neutron scattering (INS) and proton nuclear magnetic resonance (NMR), and analyzed to extract the rotational potential energy surfaces characteristic of the methyl groups in the host-guest complex. The number and relative intensities of the tunneling peaks observed by INS indicate the presence of methyl-methyl coupling interactions in addition to the methyl-zeolite interactions. The INS tunneling spectra from the crystals (space group $P2_12_12_1$ with four crystallographically inequivalent methyl rotors) are quantitatively interpreted as a combination of transitions involving two coupled methyl rotors as well as a transition involving single-particle tunneling of a third inequivalent rotor, in a manner consistent with the observed tunneling energies and relative intensities. Together, the crystal structure and the absence of additional peaks in the INS spectra suggest that the tunneling of the fourth inequivalent rotor is strongly hindered and inaccessible to INS measurements. This is verified by proton NMR measurements of the spin-lattice relaxation time which reveal the tunneling characteristics of the fourth inequivalent rotor. © *2004 American Institute of Physics.* [DOI: 10.1063/1.1781119]

I. INTRODUCTION

Crystalline nanoporous aluminosilicates (zeolites)[1,2] are used in organic separations owing to their shape and size selectivity for various types of organic sorbate molecules.[3] This behavior is influenced by the framework-sorbate and sorbate-sorbate interactions, which determine the molecular adsorption and transport processes in the porous material. Experimental techniques for studying these interactions have included NMR spectroscopy,[4,5] vibrational (Raman/IR) spectroscopy,[6] and inelastic and quasielastic neutron scattering (INS and QENS).[7–9] The neutron scattering technique is particularly advantageous in several situations, where it permits a relatively direct interpretation of the experimental observations in terms of the microscopic physical parameters such as local potential energies or molecular diffusivities. This kind of experimental information is also valuable as input for parametrizing atomistic models,[10,11] which can then be used in force-field based simulations of a wide range of material properties.

The rotational tunneling of molecules, functional groups, or ions such as H_2, CH_4, $—CH_3$, $—NH_2$, or NH_4^+ is known to be a sensitive and quantitative probe of the local energetics and structure of a material. It is most often observed[12] by INS or NMR measurements. The low-temperature quantum mechanical behavior of these rotorlike species confined in a potential well includes dynamics such as rotational tunneling and libration (torsional oscillation). The tunneling of a rigid molecular rotor such as a methyl group is very sensitive to the shape (including the rotational symmetry) and amplitude of the potential energy surface along the tunneling trajectory.[12] A methyl group attached to a larger moiety in a solid can often be approximated as a one-dimensional rotor. Considering the large incoherent scattering cross section of the hydrogen atoms, and if rotor-rotor or rotation-translation couplings (cf. Sec. III C) are negligible, the methyl group can be well approximated as a single-particle interacting with the neutron probe. In such a case, the rotational potential experienced by the methyl group is expressed as a function of a single variable, the rotation angle. This potential must have at least the threefold rotational symmetry of the methyl group about the rotation axis passing through the carbon atom and perpendicular to the plane of the three protons. The rotational potential may have higher symmetry, depending upon the local environment of the rotor. For example, the methyl rotational potential in an

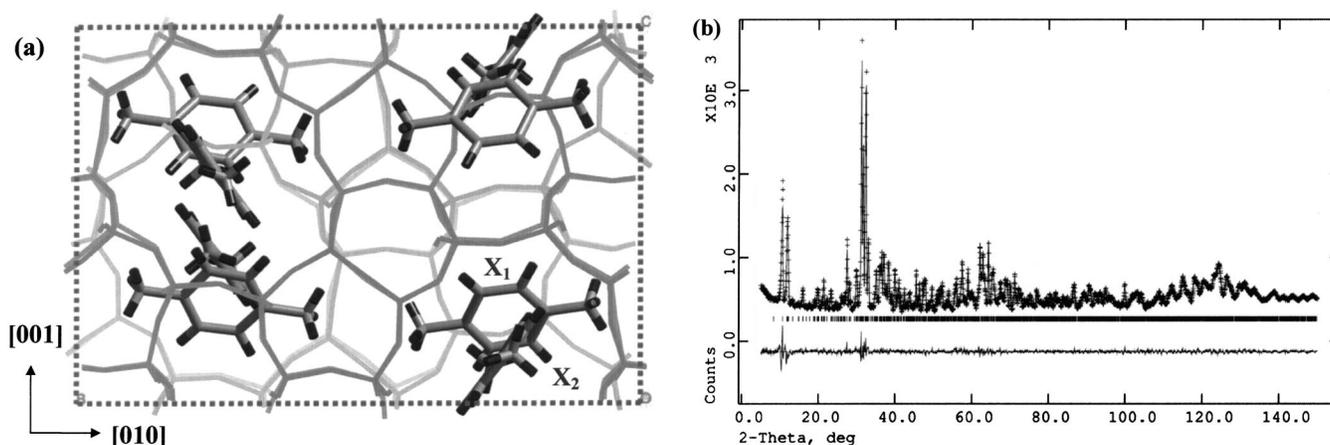[a)]Electronic mail: sankar.nair@chbe.gatech.edu

FIG. 1. (a) Unit cell of the MFI/*p*-xylene complex as viewed down the [100] direction, showing the zeolite lattice and the *p*-xylene molecules adsorbed in the crystal. (b) Powder neutron diffraction pattern of MFI/*p*-xylene complex (sample S4, Table I) showing the experimental data (+), the calculated Rietveld best fit (solid line), $P2_12_12_1$ Bragg reflection positions (tick marks), and the difference curve (bottom). Refinement weighted residual $R_{wp} = 2.68\%$, reduced $\chi^2 = 2.77$.

isolated *p*-xylene molecule has sixfold symmetry, due to the presence of the planar C_6 ring.[10] The high sensitivity of rotational tunneling to the potential energy surface may also permit a quantification of any disorder of the tunneling groups in terms of the distribution of potential barriers experienced by the methyl groups. Such information is complementary to that obtained from diffraction techniques, which quantify atomic disorder in terms of Debye-Waller displacement factors or variations in bond distances and angles.

There is an extensive literature on methyl rotational tunneling measurements for organic and organometallic molecular crystals.[12] Investigations of rotational tunneling in porous hosts have appeared more recently,[13–16] and have provided insights into the packing and energetics of molecules such as CH_4, CH_3I, and H_2 in these materials. In this paper, we investigate the use of tunneling spectroscopy to quantitatively characterize interactions involving the methyl rotor components of guest molecules adsorbed in a crystalline nanoporous host. We have chosen the zeolite silicalite (MFI topology)[1] a highly crystalline, pure silica material with a well-defined pore structure (crystallographic pore size ~8 Å) consisting of two intersecting systems of channels.[1,17] At room temperature, the material can adsorb *p*-xylene molecules to a maximum of eight molecules per unit cell.[17] Single-crystal x-ray diffraction studies at room temperature reveal that the *p*-xylene molecules are equally distributed in two distinct adsorption sites,[17] and are referred to here as X_1 and X_2 molecules [cf. Fig. 1(a)]. The methyl groups attached to the C_6 rings of X_1 and X_2 molecules have a total of four distinct environments. This is because (a) each *p*-xylene molecule carries two methyl groups and (b) the interaction of *p*-xylene with the silicalite framework lowers the space group of the crystal from *Pnma* to $P2_12_12_1$, hence removing the symmetry relationship of two methyl groups on the same *p*-xylene molecule. The silicalite/*p*-xylene complex is an interesting and well-defined model system with a typical level of complexity expected in ordered nanoporous materials containing organic molecules. It is known that the rotational potential of a methyl group in an isolated *p*-xylene

molecule is very small (a sixfold symmetric potential of ~1.2 meV corresponding to a ground-state tunnel splitting of ~650 meV),[10,18] so that in the silicalite/*p*-xylene complex an increase in the potential can be expected to be mainly due to interactions with the host framework and other *p*-xylene molecules. As shown below, rotational tunneling spectroscopy can be applied to gain quantitative information on these interactions and distinguish different environments of the methyl groups in the structure.

II. EXPERIMENTAL DETAILS

The silicalite samples were synthesized by the method of hydrothermal reaction, according to a composition described elsewhere.[19] The reactant solution includes a silica source (tetraethylorthosilicate, Aldrich Chemicals),[20] an organic template (tetrapropylammonium bromide, Aldrich), ammonium hydroxide (Aldrich), and deionized water. Crystallization of silicalite from a clear reactant solution proceeded in Teflon-lined stainless steel high pressure autoclaves at 453 K and autogenous pressure for four days. The synthesized material (crystal size ~75 μm) was calcined in air at 773 K for 5 h to decompose and remove the template molecules from the pores. The identity and high crystallinity of the sample were verified by powder x-ray diffraction.

A typical sample for INS measurements was prepared by spreading the zeolite powder in a thin, continuous layer over half the surface area of an aluminum foil of known mass. This was kept in a sealed glass vessel with a small dish containing *p*-xylene (99.9+%, Aldrich) for 48 h. The mass of the zeolite was measured before and after adsorption to calculate the loading of *p*-xylene. The other half of the aluminum foil was then quickly folded over the zeolite layer and closed at the edges to obtain a waferlike sample. This wafer was immediately inserted as the inner lining of a cylindrical aluminum sample can (with an indium wire seal) and cooled to the measurement temperature (10 K) in a closed-cycle refrigerator. For powder neutron diffraction measurements, deuterated *p*-xylene (C_8D_{10}, 99.9+%, Aldrich) was ad-

TABLE I. Sample masses (excluding Al foil) and *p*-xylene loadings.

Sample no.	Mass before adsorption (g)	Mass after adsorption (g)	*p*-xylene loading (molecs/unit cell)
S1	5.16	5.87	7.48
S2	3.18	3.63	7.69
S3	2.65	3.00	7.18
S4[a]	6.08	7.02	7.68

[a]Loaded with deuterated *p*-xylene.

sorbed in silicalite. In this case the sample was packed (in bulk) into a vanadium can after adsorption, and no aluminum foil was used. Table I shows a list of these samples and the loading of *p*-xylene expressed as the number of molecules per unit cell. Neutron scattering measurements were conducted at the NIST Center for Neutron Research with the NG-2 high flux backscattering spectrometer (HFBS), the NG-4 disk chopper time-of-flight spectrometer (DCS), and the NG-6 Fermi chopper time-of-flight spectrometer (FCS). The measured data were reduced using the DAVE package,[21] which allows normalization to the beam monitors, application of a detector efficiency correction with a vanadium standard, grouping of detector intensities, and calculation of the neutron absorption factors. Data fitting was carried out with the peak analysis utility in DAVE. Neutron diffraction data were measured on the NIST BT-1 diffractometer with a Ge311 collimator. The data were analyzed by the Rietveld refinement technique using the GSAS[22] and EXPGUI[23] programs. NMR measurements between 4 and 180 K were conducted at the University of Nottingham on the field-cycling NMR spectrometer, operating at a Larmor frequency of 42.6 MHz and a magnetic field strength of 1 T. The precision of temperature control was better than 1 K.

III. RESULTS AND DISCUSSION

A. Crystal structure

Figure 1(a) shows the unit cell of the silicalite/deuterated *p*-xylene complex, obtained by Rietveld refinement using the neutron powder diffraction pattern measured at 10 K [Fig. 1(b)] from sample S4. Most aspects of the room-temperature structure are already known from a previous single-crystal x-ray diffraction study[17] and are not reported in detail here. In the present study, we refine the coordinates for the structure at 10 K, and obtain the locations of the deuterium atoms of the methyl groups. For this purpose, the refinement was carried out using tetrahedrally symmetrized "semirigid" methyl groups with fixed D-C-D bond angles of 109.47°, but a single refinable C-D bond length for each methyl group.[24] The locations of the 24 inequivalent silicon and 48 inequivalent oxygen atoms are refined initially. A single isotropic Debye-Waller factor (U_{iso}) is used for all framework atoms of the same element. The carbon atoms of the same *p*-xylene molecule are treated with a single U_{iso}, and the deuterium atoms attached to the C_6 rings are treated similarly. All three deuteriums on the same —CD_3 group are assigned the same U_{iso}. The occupancy of all atoms is taken as unity, as dictated by the ideal chemical composition and the crystal structure, and only the locations and U_{iso} are refined. This is rea-

sonable since the zeolite is highly crystalline with few defects, and the *p*-xylene sites are almost fully occupied (Table I).

The structure contains an intersecting system of linear pore channels propagating along [010] and sinusoidal pore channels along [100]. Some quantitative results of the structure refinement are summarized in Table II. The silicon atoms and the C_6 atoms in the *p*-xylene molecules maintain the expected bond geometries based on their respective sp^3 and sp^2 hybridizations. The *p*-xylene molecules, however, have larger Debye-Waller factors than the silicalite framework, indicating that any disorder effects in the tunneling spectra would mainly be due to positional disorder in the adsorbed *p*-xylene molecules. A slightly lower actual occupancy of the *p*-xylene molecules (the maximum value being four molecules each per unit cell for X_1 and X_2) may also contribute to a higher Debye-Waller factor. The methyl groups appear to have essentially the same C-D bond lengths within experimental error; however, even small variations in the bond lengths may appreciably influence the tunnel splittings.[10] In agreement with previous studies, it is clear that a chain of *p*-xylene molecules X_1 is adsorbed along the linear channel. The methyl rotors (M_1 and M_2) of adjacent molecules face each other at a C···C distance of 4.15(4) Å. The long axis of X_1 is slightly tilted by 10.1(5)° from the [010] axis. The other *p*-xylene molecule X_2 (carrying methyl groups M_3 and M_4) is adsorbed in a channel of sinusoidal shape propagating along the [100] direction. These methyl groups do not face each other, but interact with the C_6 rings of the molecules X_1 [also cf. Fig. 2(c)].

The deuterium atoms of the methyl groups are found to be quite localized. By rotating the methyl groups to different initial orientations, we obtained convergence to only one orientation for each methyl group that leads to the best fit of the diffraction pattern. Figure 2(a) shows the nuclear densities in the vicinity of the two methyl groups M_1 and M_2, which are located on adjacent *p*-xylene molecules and are facing each other approximately in the [010] direction. These are calculated based on the observed intensities taken from the powder pattern and the phases from the crystal structure after completion of the refinement. The difference maps in this region are featureless. We also find that M_1 and M_2 are not oriented precisely parallel to each other. Instead, M_2 is staggered at a rotation angle of ≈35° with respect to M_1 when viewed down [010]. Figure 2(b) shows the environment of each of the four methyl rotors in the host framework, along with the closest distances to the framework oxygens for each of the protons. Based on these contact distances, it appears that the rotors M_3 and M_4 are somewhat more tightly confined in the ten-membered silicate rings of the zeolite host than are rotors M_1 and M_2. While the *p*-xylene molecules on site X_1 are arranged in a linear chainlike fashion, a molecule on site X_2 does not interact strongly with another X_2 site but rather with two adjacent X_1 sites, as shown in Fig. 2(c) with the zeolite framework removed for clarity. We discuss this arrangement in more detail in Sec. III E.

TABLE II. Summary of structural details of the MFI/deuterated *p*-xylene complex at $T = 10$ K.

Space group: Orthorhombic $P2_12_12_1$ (No. 19)
Lattice constants (Å): $a = 20.1130(3)$, $b = 19.7887(4)$, $c = 13.4081(3)$

Silicalite framework				
Si-O distance (Å)	*mean* 1.598(10)		*SD* 0.007(1)	
O-Si-O angle (angle)	109.5(11)		1.6(1)	
Si-O-Si angle (angle)	153.9(12)		9.6(1)	
$U_{Si}(Å^2) \times 100$	0.05(7)		N.A.	
$U_{O}(Å^2) \times 100$	0.60(3)		N.A.	

C_6 *rings*	X_1		X_2	
C-C distance (Å)	1.42(1)	0.05(0)	1.43(1)	0.05(0)
C-D distance (Å)	1.03(2)	0.02(0)	1.05(2)	0.03(0)
C-C-C angle (deg)	120.7(1)	2.7(1)	119.8(1)	2.3(1)
C-C-D angle (deg)	118.8(2)	4.5(1)	120.0(1)	2.6(1)
$U_C(Å^2) \times 100$	3.13(18)	N.A.	2.36(16)	N.A.
$U_n(Å^2) \times 100$	4.71(34)	N.A.	4.45(29)	N.A.

Symmetrized-CD_3	M_1	M_2	M_3	M_4
C-D distance (Å)	1.03(2)	1.03(2)	1.07(2)	1.02(3)
$U_D(Å^2) \times 100$	6.53(53)	5.46(47)	4.37(43)	4.24(43)

B. INS measurements

Figure 3(a) shows the INS spectrum obtained from sample S1 at 10 K on the disk chopper time-of-flight spectrometer NG-4 (DCS), with an incident neutron wavelength of 9 Å. The data are summed over Q values of 0.45–1.3 Å^{-1}. At this wavelength, the instrumental resolution ($\sim$22 μeV) is enough to resolve two inelastic peaks. The spectrum was initially fitted with two pairs of Lorentzian peaks, a δ function for the elastic scattering, and a sloping background, all convoluted with the instrumental resolution function. The resolution function was obtained by fitting the elastic line from a silicalite sample (with no *p*-xylene adsorbed). The preliminary fit also indicated the possible presence of a third inelastic peak quite close to the elastic line. This may as well arise from the fact that the resolution function displays a low-intensity tail near the elastic peak which is difficult to capture satisfactorily during a fit of the elastic line from the silicalite sample. We include a third pair of Lorentzians to fit this peak, but we regard its assignment to a tunneling peak as speculative at this stage. Figure 3(a) shows the subsequent best fit of the three pairs of Lorentzians. In the case of methyl rotors adsorbed in disordered porous materials, a Gaussian distribution of potential barriers leads to a log normal (asymmetric) energy transfer line shape.[13,15,25] We found it difficult to fit log normal line shapes to the inelastic scattering data. This is possibly because the present material is crystalline, and hence there may not be a Gaussian distribution of potential barriers for the methyl groups of *p*-xylene in silicalite. Additionally, the potential energy barriers in this case (cf. Sec. III C) may be close to the limits of validity (50–1000 K) of the expression proposed earlier[25] relating the tunneling energies to the barrier heights, which leads to an asymmetric energy transfer line shape. Here we use Lorentzian (symmetric) line shapes since they provide a good fit to the experimental data, while leaving the question of the shape of the potential barrier distribution to a later investigation. From the fit of Fig. 3(a), we obtain three peaks with

energies of 226(4), 124(2), and 40(1) μeV and full width half maxima (FWHM) of 192(2), 78(2), and 16(2) μeV, respectively (cf. Table III).

Figure 3(b) shows the spectrum measured on the backscattering spectrometer NG-2 (HFBS) at 10 K, using sample S2. The data are summed over the same Q values (by including detectors 3–12) as the data of Fig. 3(a). An energy range of $\pm$36 μeV has been used, and the energy resolution is $\sim$1 μeV. There is a single pair of broad peaks in the spectrum. There is no evidence of a peak near 40 μeV, and hence the 40 μeV peak fitted in the NG-4 spectrum is the tail of the resolution function rather than a tunneling peak. The data are fit by a δ function, a flat background, and a pair of Lorentzian functions convoluted with the resolution function. The obtained tunnel splitting is 9.8(1) μeV, with a FWHM of 12.5(5) μeV. In order to express the intensity of this peak on approximately the same scale as the peaks observed on NG-4, we multiply its fitted intensity by the following scale factor f:

$$f = \left(\frac{\alpha_{NG-4}}{\alpha_{NG-2}^2} \right) \left(\frac{M_{NG-4}}{M_{NG-2}} \right). \quad (1)$$

Here α is the neutron absorption factor which depends on the incident wavelength, the sample composition, and sample can geometry, whereas M is the mass of the sample used (Table I). In the backscattering spectrometer NG-2, the neutron beam passes through the sample twice, so that α has to be squared. To a good approximation, no other corrections should be necessary since the data have been summed over the same Q range, the background has been accounted for in the fits, and the data are normalized in all cases to the beam monitors (and hence to the counting time) as well as to a vanadium standard. To calculate the neutron absorption factors, we assume that the powder samples are distributed evenly on the inside surface of the sample can (of known geometry). Since the compositions of the samples are known, the effective scattering lengths and wavelength-
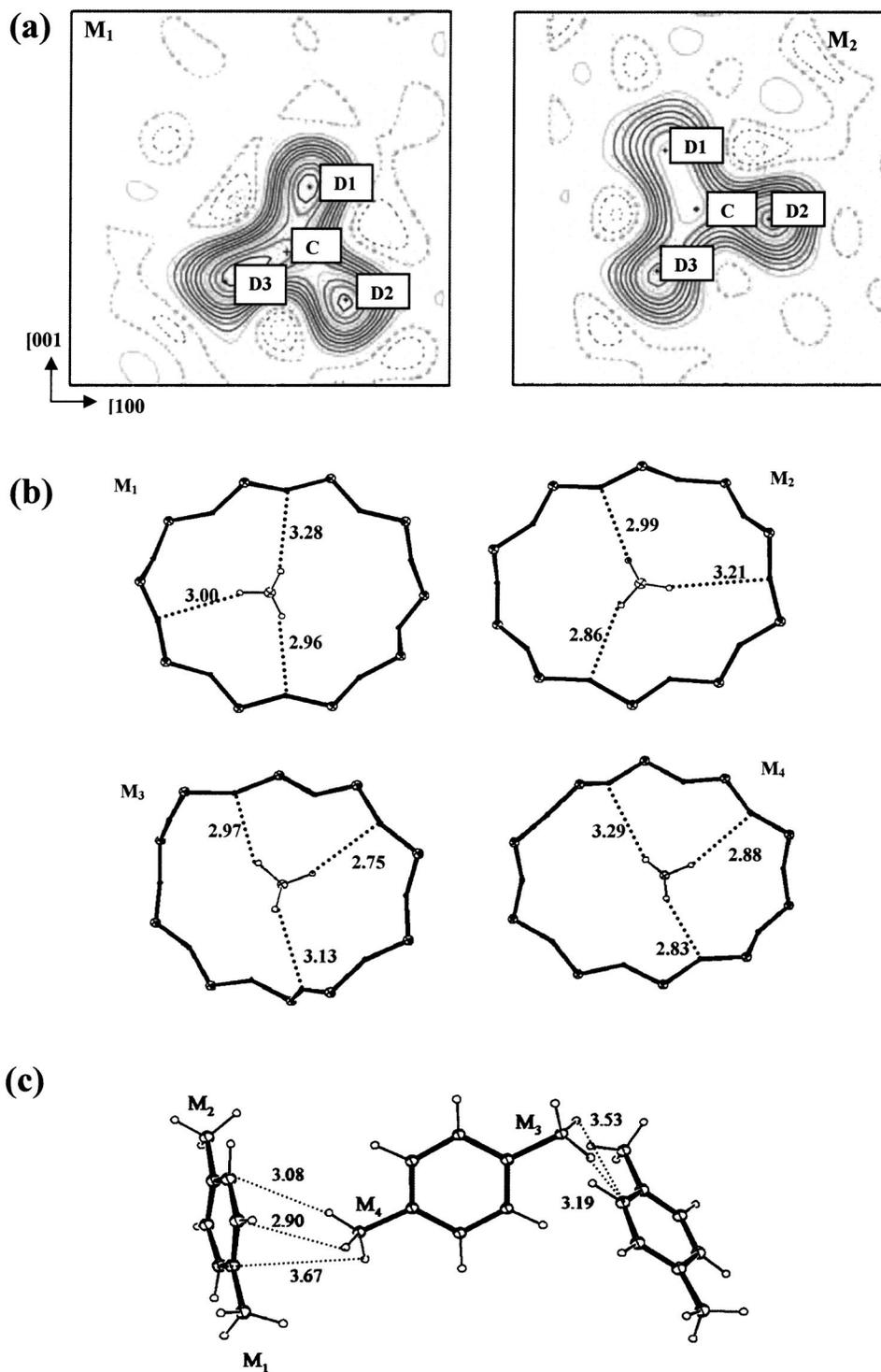
FIG. 2. (a) Cross section (viewed down [010]) of observed nuclear number density maps (5×5 Å^2) for methyl groups M_1 and M_2. The contours on these maps range from -0.3 to 1.1 Å^{-3}. Contours of negative density are shown by dashed lines. The M_1 map is centered on fractional coordinates $(x,y,z) = (0.5, 0.4, 0.25)$ and the M_2 map on $(x,y,z) = (0.5, 0.572, 0.25)$. (b) Environment of methyl rotors $M_1 - M_4$ in the zeolite framework based on the refined crystal structure. The closest distances (Å) to the framework oxygens are indicated. (c) Arrangement of three *p*-xylene molecules in the crystal. The shortest distances between the protons of methyl groups M_3 and M_4 to the carbon atoms of the C_6 rings are indicated. No other *p*-xylene molecules are close enough to interact directly with the molecule X_2 shown in the center.

dependent absorption lengths are easily calculated. The absorption factors are then estimated for the annular samples of known geometries as implemented in the program DAVE. These values are $\alpha = 0.74(7)$ for S1 and $0.79(8)$ for S2.

Table III shows the list of peak parameters extracted

from the spectra of Figs. 3(a)–3(b). The relative intensities do not suggest that the single-particle model of tunneling is valid for this system. The single-particle tunneling of four inequivalent methyl groups would lead to four tunneling peaks of equal intensity, which is not observed here. There-
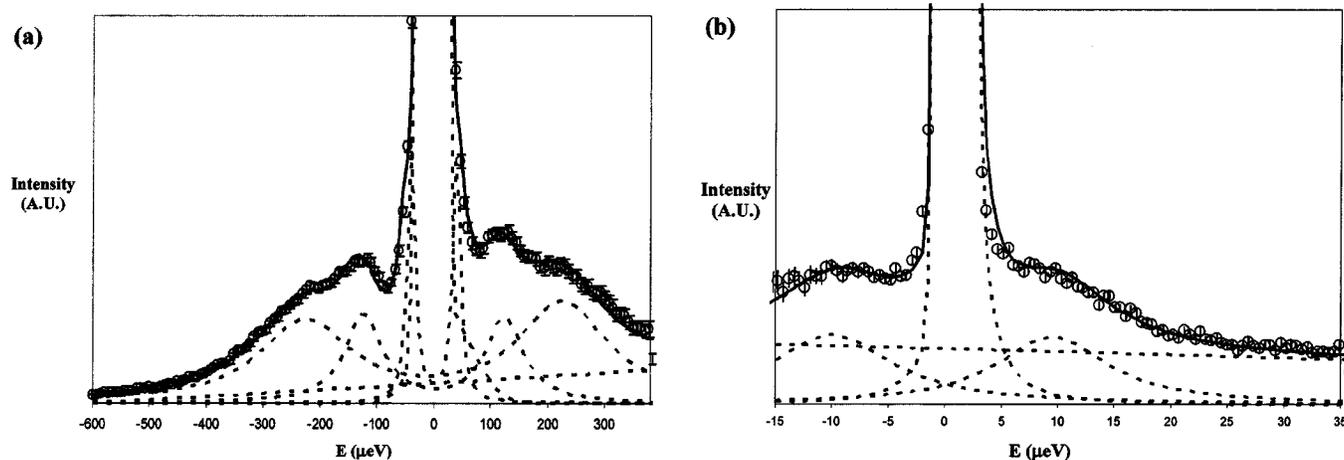
FIG. 3. (a) Inelastic neutron scattering spectrum measured at 10 K on NG-4 for sample S1. The circles show the experimental data, the solid line is the total fit, and the dashed lines indicate the five components (δ function, sloping background, and three pairs of lorentzians) of the fit, convoluted with the resolution function obtained from a blank silicalite sample. (b) Inelastic neutron scattering spectrum measured at 10 K on NG-2 for sample S2. The circles show the experimental data, the solid line is the total fit, and the dashed lines indicate the three components (δ function, flat background, and a pair of Lorentzians) of the fit, convoluted with the resolution function obtained from a blank silicalite sample.

fore, we look to the crystal structure to indicate possibilities for interactions between the methyl groups that cause deviations from the single-particle model. The likely candidates are the two methyl groups M_1 and M_2 which, as mentioned earlier, are facing each other in the straight channel of the zeolite with a C$\cdots$C distance of 4.15 Å. Rotor coupling effects have been suggested to influence the methyl tunneling spectra in some organometallic crystals,[26,27] where they cause peak broadening and the appearance of additional peaks not explained by the single-particle model. However, such effects can also be produced by the coupling of a single rotating methyl group to its translational degrees of freedom, and in the case of lithium acetate[27,28] it provides an alternative to the coupled-rotor model. The coupled-rotor model can be parametrized purely from experimental data, since the potential expressions are functions only of the rotational angles. On the other hand, the translational-rotational coupling model requires expressing the crystal potential in terms of both the translational and rotational coordinates, leading to a considerable increase in the number of parameters. These have to be estimated by force-field based calculations,[28] or from nuclear density maps obtained from single-crystal neu-

tron diffraction data.[29] In the present case, we investigate how well the rotor-rotor coupling model assists in explaining the observed spectra, since the crystal structure suggests the possibility of such coupling effects. Figure 2(a) also hints that in this system, rotor-rotor coupling is more likely than rotation-translation coupling. This is because the nuclear densities of the methyl groups retain threefold symmetry, whereas in the case of lithium acetate[28] and nickel hexammine salts[29] the rotation-translation coupling disorders the protons/deuterons and alters their rotational symmetry as observed by neutron diffraction. Although the crystal structure indicates that the rotors M_1 and M_2 are not precisely coaxial (the projection of the C$\cdots$C distance on the XZ plane in Fig. 2(a) is about 1 Å), the fact that they are separated by a C$\cdots$C distance of 4.15 Å allows us to treat the two rotors as approximately coaxial.

C. Extraction of potential energy parameters

The rotational potential acting on a single methyl group causes the splitting of its librational ground state into a nondegenerate A symmetry and a twofold E symmetry state of the spatial part of the wave function. The spin symmetry (A or E) of these states is dependent on the spatial symmetry, since the wave function (expressed as a product of space and spin components) must be invariant under permutation of the three protons.[30] For two distinguishable, coupled methyl rotors (labeled a and b), the librational ground state splits into a single AA level (with the lowest energy), a fourfold AE (or EA) level, a twofold E_aE_b (or E_bE_a) level, and a twofold E_aE_a (or E_bE_b) level.[27,30,31] If the rotor-rotor coupling is reasonably strong in relation to the single-particle component of the potential, the splitting between the E_aE_b and E_aE_a levels can be large enough to be observed with INS. The allowed transitions[31] in the ground-state multiplet are $AA \rightarrow AE$ (energy E_{01}), $AE \rightarrow E_aE_b$ (E_{12}), $AE \rightarrow E_aE_a$ (E_{13}), and $E_aE_b \rightarrow E_aE_a$ (E_{23}). Typically, the energies for the first three transitions are clustered together in INS spectra with

TABLE III. Peak parameters extracted by least-squares fitting from the INS spectra.[a] The estimated errors are given as uncertainties in the last reported decimal digit. The calculated relative intensities (cf. Sec. III D) are also shown.

Energy[b] (μeV)	FWHM (μeV)	Intensity ($\times 10^3$)	Scale factor f [Eq. (1)]	Relative intensity (expt.)	Relative intensity (calc.)
226(2)	192(2)	3.88(17)	1	1	1
124(1)	78(2)	1.50(8)	1	0.39(4)	0.46
9.8(1)	12.5(5)	0.17(3)	1.92	0.08(7)	0.16

[a]A fourth peak at 40 μeV extracted from the NG-4 (DCS) spectrum was determined to be spurious by comparison to the NG-2 (backscattering) results.

[b]For comparison, the methyl tunnel splitting in an isolated *p*-xylene molecule is ~650 μeV (Ref. 18).

E_{01} having the highest intensity, whereas the energy and intensity of the fourth transition (E_{23}) are considerably smaller. For the system of two coaxial methyl rotors facing each other, with their rotation angles (α_1 and α_2) measured about the same rotation axis, the two-particle Hamiltonian is

$$H = -B\left(\frac{\partial^2}{\partial \alpha_1^2} + \frac{\partial^2}{\partial \alpha_2^2}\right) + V(\alpha_1) + V(\alpha_2) - W(\alpha_1, \alpha_2). \quad (2)$$

The first term in parentheses is the kinetic energy operator. B ($= \hbar^2/2I$) is the rotational "constant" of the methyl group [often taken as 655 μeV (Refs. 10 and 12)], and depends on the moment of inertia I of the methyl group about the rotation axis. The single-particle component of the potentials can be approximated as having the same magnitude (but different phase factors) for both rotors M_1 and M_2, since their crystallographic inequivalence is a result of slight changes in relative position during the $Pnma$ $\rightarrow P2_12_12_1$ phase transition.[17] We use threefold symmetric functions $V(\alpha_1) = (V_3/2)[1 - \cos 3\alpha_1]$ and $V(\alpha_2) = (V_3/2) \times [1 - \cos 3(\alpha_2 + \phi)]$ as the single-particle potentials. Here, ϕ is a phase factor. A sixfold symmetric term with magnitude V_6 can be added (or substituted) to describe the single-particle potential. The last term is the coupling potential which depends on the relative rotation angle of the two rotors and is taken to be threefold symmetric in the simplest approximation, i.e., $W(\alpha_1, \alpha_2) = (W_3/2)[1 - \cos 3(\alpha_1 - \alpha_2)]$. The total potential energy $V(\alpha_1, \alpha_2)$ in Eq. (2) is the combination of the three terms above.

The sign of V_3 can be arbitrarily chosen as positive. In the absence of rotor-rotor coupling, and if the two rotors were in phase (i.e., $\phi = 0$), the single-particle potential tends to orient the two rotors in parallel, with the energy minimum at $V(0,0) = 0$. The coupling term tends to stagger the two rotors with a relative angle of 60°. Hence, the potential energy minimum can only be at $V(0,0) = 0$ or $V(0,60°) = V(60°,0) = V_3 - W_3$, depending on the relative magnitudes of the single-particle and coupling terms. The introduction of the phase factor ϕ allows the minimum to fall at intermediate orientations. It can be shown that if $V_3 > W_3 > 0$, the minimum occurs at $V(0, -\phi) = (-W_3/2)[1 - \cos 3\phi]$. We find from Fig. 2(a) that the coupled rotors retain threefold symmetry in their nuclear densities. This argues against the use of sixfold symmetric single-particle potentials, except in the unlikely case where the threefold coupling term is much larger than the single-particle terms. Even then, the rotors would prefer a relative angle of 60°, which is not observed. Hence, we only consider threefold symmetric potentials in this paper.

Based on the tunnel splittings and intensities in Table III, the broad, intense peak at 226 μeV and the much less intense peak at 9.8 μeV are likely to arise from rotor-rotor coupling effects. Since the energies E_{01} and E_{23} are expected to be in different regions of the spectrum, we extract preliminary values of V_3 and W_3 by assuming that $E_{23} = 9.8 \mu$eV and the ground-state transition $E_{01} = 226 \mu$eV. We first obtain energy eigenvalues and two-particle spatial wave functions for a large number of potential parameter values, the Hamiltonian being given by Eq. (2) with the two rotors being in phase ($\phi = 0$). The wave functions are expressed as expan-

sions of free-rotor basis functions of the form $(1/2\pi)e^{im\alpha_1}e^{in\alpha_2}$ ($m, n = 0, \pm 1, \pm 2, ...$).[27] The size of the resulting Hamiltonian matrix is truncated at 441×441 because no significant increase in accuracy is obtained by further increasing the matrix size. From the obtained energy eigenvalues, we can calculate the first four allowed transitions. In the parameter space studied ($0 \leq V_3 \leq 50B$, $-50B \leq W_3 \leq 50B$), we obtain $(V_3, W_3) = (21.6B, 14.2B)$. Assuming $B = 655 \mu$eV, we have $V_3 = 14.2$ meV and $W_3 = 9.3$ meV. The corresponding values of E_{12} and E_{13} are calculated as 237 and 246 μeV, respectively. Clearly, the first three transitions are closely clustered in the same region of the tunneling spectrum, which is also consistent with the apparent breadth of this peak in Fig. 3(a). However, since $V_3 > W_3$, this potential would lead to a parallel alignment of the two rotors. Therefore, we attempt to refine the potential by introducing the phase factor $\phi = -35°$ in accordance with the observed arrangement of the methyl groups M_1 and M_2. In this case we obtain $V_3 = 6.9$ meV and $W_3 = 6.2$ meV. The corresponding values of E_{12} and E_{13} are 203 and 216 μeV, respectively. If we assign the remaining tunneling peak at 124 μeV to either one of the methyl groups M_3 and M_4 in the sinusoidal channels (which are not coupled to other rotors), the corresponding threefold single-particle potential is $V_3 = 12.2$ meV. This potential is stronger than that experienced by the methyl rotors in the straight channels, and indicates stronger interactions of these methyl groups with the crystal structure. These parameters also appear to be consistent with the librational density of states obtained from sample S3 on the NG-6 spectrometer (FCS) at an incident wavelength of 2.48 Å and $T = 6.8$ K. These data indicate a group of librational transitions in the region 4–8 meV, in approximate agreement with the librational transitions predicted from the potential expressions with the coupled-rotor parameters (6.9 meV, 6.2 meV; $\phi = -35°$) and the single-rotor parameters (12.2 meV, 0.0 meV). However, the librational measurements are not conclusive, since the error bars in our librational spectra on NG-6 indicated that an unreasonably long measurement time would be required to obtain statistically valid data.

D. Spectral intensities

The interpretation of the observed tunneling spectrum can also be aided by calculations of the tunneling intensities. We have performed these calculations for the methyl groups $M_1 - M_4$ based on their geometries as derived from the crystal structure and using the potential energy parameters extracted from the tunneling spectra. The methodology for these calculations is described in detail in previous works.[28–32] Briefly, the intensity of a transition of the methyl rotor (or system of two coupled rotors) from an initial state $|i\rangle$ to a final state $|f\rangle$ is directly proportional to the matrix element $\Sigma_{\mu,\nu}|\langle\nu|\langle f|W|i\rangle|\mu\rangle|^2$, where $|\mu\rangle$ and $|\nu\rangle$ are the initial and final spin states of the neutron and the summation reflects the use of an unpolarized neutron beam. The operator W is the sum of the interaction operators $SI(j)e^{i\vec{Q}\vec{R}(j)}$ over all the protons j; S being the spin operator of the neutron, $I(j)$ the spin operator of the jth proton, $\vec{R}(j)$ its position, and $\hbar\vec{Q}$ the momentum transfer. For the coupled rotor system

(M_1, M_2) we calculate the intensity based on the geometry of two coaxial rotors facing each other with a C···C distance of 4.15 Å and C-H bond lengths of 1.03 Å (Table II). The position vectors of the six protons are calculated from this geometry. The spatial components of the initial and final wave functions (within the ground-state multiplet) are obtained as the eigenfunctions of the Hamiltonian matrix [Eq. (2)]. The ''raw'' eigenfunctions obtained by diagonalization of the Hamiltonian matrix are properly symmetrized by applying the projection operators[32] based on the nine symmetry operations of the Abelian group $C_3 \times C_3$ (which describes the rotational symmetry of the two-rotor system). The spin part of the wave functions of the six protons can be written in terms of 2^6 basis functions. For any given spatial symmetry, the spin symmetry is determined by applying the condition that the spin-dependent wave function must be totally symmetric under the group operations. Hence the spin part of the wave function is generated by applying the projection operator to any of the basis functions with the appropriate symmetry. In evaluating the matrix elements, the required integrals[32] over the rotation angles and over the solid angle (for powder averaging of the intensities) are calculated numerically by multidimensional quadrature.

The resulting relative intensities for the four allowed transitions of energies E_{01}, E_{12}, E_{13}, and E_{23} (Sec. III C) are practically constant in the Q range (0.45–1.3 Å^{-1}) used for the present experiments and are in the ratio 1:0.59:0.59:0.34. If we consider the broad peak in Fig. 3(a) (with the fitted tunnel splitting of 226 μeV) as including three closely spaced transitions E_{01}, E_{12}, and E_{13} (Sec. III C), then the calculated ratio of the total intensity of this composite peak to that of the peak assigned to E_{23} would therefore be 1:0.16. This is in fairly good agreement with Table III, which shows a corresponding experimental intensity ratio of 1:0.08(7). If we consider the peak at 124 μeV as due to either M_3 or M_4, then the calculated intensity ratio of this peak to the broad composite peak is 0.46:1. This is again in good agreement with Table III, which shows a corresponding experimental intensity ratio of 0.39(4):1. This is further evidence for the assignment of tunneling peaks from the coupled methyl rotors M_1 and M_2.

E. NMR measurements

Two problems remain in the interpretation of the INS tunneling spectrum, i.e., the assignment of the peak at 124 μeV to the correct methyl rotor M_3 or M_4 and an explanation for the absence of tunneling intensity from the remaining methyl group. In addressing these problems, we examine the arrangement of *p*-xylene molecules in the zeolite, as shown in Fig. 2(c) with the zeolite framework removed for clarity. The methyl rotors M_3 or M_4 of the *p*-xylene molecule X_2 interact differently with the C_6 rings of two adjoining *p*-xylene molecules X_1. The protons on M_4 could interact quite strongly with the π electrons[17] due to the several short C···H distances [Fig. 2(c)] and because the C_6 ring faces towards this methyl group, whereas this interaction would be much smaller for M_3 since the C_6 ring faces away from it. Due to the possibility of a strong M_4-X_1 interaction,

we hypothesize that the tunneling barrier for M_4 is too high (and the tunnel splitting too low, below 1 μeV) to be measured with INS. Therefore, we can tentatively assign the observed tunneling peak at 124 μeV to the methyl rotor M_3, whereas the rotational tunneling of M_4 should be observable by NMR which can probe the relevant energy window.

Figure 4 shows the temperature dependence of the spin-lattice relaxation time[33] T_1 of the protons as measured by NMR. The measurement of T_1 samples the spectral density at the particular NMR frequency. Minima in the temperature dependence of T_1 are observed when the time scale of a molecular motion involving the protons matches the time scale of the NMR frequency, 42.6 MHz. In the MFI/*p*-xylene complex, such molecular motions correspond to methyl rotational tunneling at low temperatures wherein the C_6 rings of the *p*-xylene molecules are frozen in their adsorption sites. A zeolite sample after exposure to *p*-xylene vapor (cf. Sec. II) was cooled down to 14 K in the NMR temperature control stage to prevent any significant loss of *p*-xylene molecules from the crystal. The spin-lattice relaxation time was measured from 14 to 180 K. Then the sample was cooled down to 14 K for low temperature measurements from 14 to 4 K. Figure 4 shows a broad minimum centred at ~8 K. A sharper drop in T_1 is seen in the 20–50 K range. Beyond 50 K, the relaxation time drops steeply as the temperature increases, so that the minimum at intermediate temperatures (20–50 K) appears as a shoulder in the data of Fig. 4.

The experimental data were fitted by a model[33,34] that expresses the relaxation time in terms of the tunneling parameters shown in Table III. For the weakly hindered methyl rotors M_1–M_3, the model gives a good description of the low-temperature part of the T_1 data. Due to the disordered tunneling as well as the coupling between the rotors, the broad composite minimum could not be experimentally resolved to reveal the details of rotational tunneling of each rotor. The effective activation energy for the tunneling of these rotors is found to be 3 ± 0.4 K (0.26 ± 0.03 meV or 25 ± 3 J/mol). This is estimated by fitting the slopes on either side of the broad feature with an Arrhenius temperature dependence and averaging the two slopes. We attribute the shoulder at intermediate temperature to the rotational tunneling of methyl rotor M_4. The corresponding single-particle tunneling barrier height, estimated from the well established correlation curve due to Clough,[35,36] is $V_3 = 86.3$ meV. This increased barrier height is consistent with the hypothesis of a strong M_4-X_1 interaction, and is outside the single-particle tunneling barrier range probed by NG-2 (20–50 meV). We therefore regard this feature in the NMR data as direct evidence of the tunneling of the fourth inequivalent rotor. The estimated activation energy 7.8 meV of the T_1 shoulder feature is somewhat less than that expected for a threefold symmetric methyl group with this barrier height; this is not surprising given the overlap with the contributions from the weakly hindered methyl groups and the degree of disorder that is apparent from the low temperature INS experiments. Figure 4 shows the individual fit components (other than the high-temperature feature beyond 50 K) and the total fitted curve which compares well with the experimental data. The
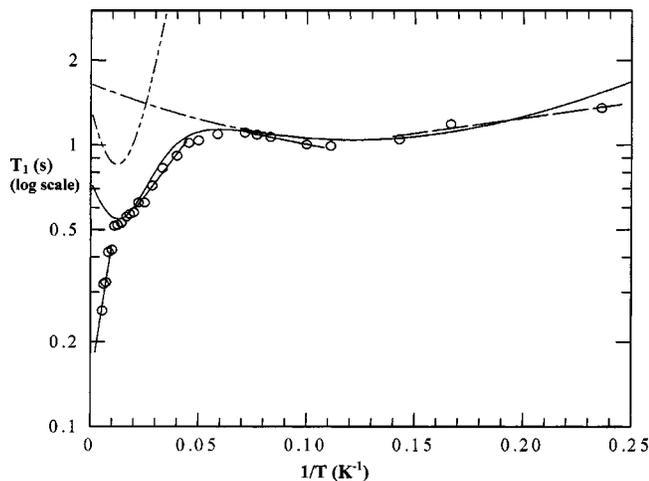
FIG. 4. Temperature dependence of the proton spin-lattice relaxation time (T_1) as measured by NMR (42.6 MHz). The experimental data are shown as open circles on a semilog scale vs the reciprocal of the temperature. The fitted slopes of various regions of the curves (cf. Sec. III E) are shown as straight lines. The two predicted components of the T_1 curve at low and intermediate temperatures are shown, and their sum is superposed on the experimental data.

high temperature drop in the relaxation time may be due to reorientations of the entire *p*-xylene molecules, as suggested by recent experiments.[5] It was suggested that this type of motion can occur by a combination of translation and rotation of *p*-xylene molecules in the void spaces at the intersections of the straight and the sinusoidal channels. We also mention that in a preliminary NMR experiment, we observed some nonreproducibility in the scale of T_1 upon temperature cycling, even though the tunneling features remained the same. This may be due to a fault in the heater (which caused the sample to warm up to room temperature and hence would have led to some desorption from the sample), or due to some type of annealing of the structure upon temperature cycling. However, no evidence for annealing effects was found in a subsequent experiment that produced the data presented in Fig. 4.

IV. CONCLUSION

The methyl rotational tunneling spectrum of *p*-xylene confined in a crystalline nanoporous zeolite host shows effects that can be explained by a combination of single-rotor and coupled-rotor tunnelings. Based on INS measurements, the tunneling spectra have been assigned to three of the four inequivalent methyl rotors in the crystal structure of the material. Quantitative rotational potentials have been extracted from the data, and show that the coupling interactions of the methyl rotors in the straight channels of the zeolite are of the same order as the rotor-framework interactions. The methyl rotors in the sinusoidal channel appear to have a considerably lower tunnel splitting and hence higher rotational potential barriers, which indicates their stronger interaction with the crystal structure. Our assignment indicates that the tunnel splitting of one of these rotors is outside the INS regime, and this has been verified by NMR measurements of the spin-lattice relaxation time. Hence, we are able to use rotational

tunneling spectroscopy as a quantitative probe of all the different environments of the methyl groups in the crystal.

The rotational tunneling spectra also contain information on the distribution of rotational potentials experienced by the methyl groups, which is a measure of their disorder in the crystal. In contrast to mesoporous hosts with pore sizes of several nanometers,[13] the methyl groups in this system are confined in an anisotropic crystal with pores of ~1 nm in size and a periodic wall structure. Owing to the tight confinement in a crystalline host, even a small static or dynamic disorder in the locations or orientations of the *p*-xylene molecules (as characterized to a limited extent by the Debye-Waller factors of Table II) may lead to substantial broadening of tunneling peaks. In disordered mesoporous hosts, the distribution of tunneling barriers can be assumed to be Gaussian, but its functional form is not obvious in the present case of a nanoporous host whose pores have a periodic structure and are of the same order of size as the guest molecules. It may be of future interest to use tunneling spectroscopy in combination with studies of crystal structure and dynamics to obtain information regarding the barrier distributions. For example, molecular simulations based on zeolite-sorbate interatomic potentials[37,38] could be used to extract the functional forms of these distributions, which may then be fitted accurately by means of the experimental tunneling spectra. The experimentally obtained rotational potentials can also be used in refining these zeolite-sorbate potentials to include consistency with tunneling spectra,[10] which are strongly sensitive to intermolecular potentials.

[1] Ch. Baerlocher, W. M. Meier, and D. H. Olson, *Atlas of Zeolite Framework Types* (Elsevier, Amsterdam, 2001).
[2] M. E. Davis, Nature (London) **417**, 813 (2002).
[3] *Handbook of Zeolite Science and Technology*, edited by S. M. Auerbach, K. A. Carrado, and P. K. Dutta (Dekker, New York, 2003).
[4] Y. Komori and S. Hayashi, Langmuir **19**, 1987 (2003).
[5] C. A. Fyfe and A. C. Diaz, J. Phys. Chem. B **106**, 2261 (2002).
[6] Y. N. Huang, J. H. Leech, E. A. Havenga, and R. R. Poissant, Microporous Mesoporous Mater. **48**, 95 (2001).
[7] R. Mukhopadhyay, A. Sayeed, S. Mitra, A. V. A. Kumar, M. N. Rao, S. Yashonath, and S. L. Chaplot, Phys. Rev. E **66**, 061201 (2002).
[8] H. Jobic, Microporous Mesoporous Mater. **55**, 159 (2002).
[9] A. M. Davidson, C. F. Mellot, J. Eckert, and A. K. Cheetham, J. Phys. Chem. B **104**, 432 (2000).
[10] M. Prager, W. I. F. David, and R. M. Ibberson, J. Chem. Phys. **98**, 5653 (1993).
[11] E. Jaramillo and S. M. Auerbach, J. Phys. Chem. B **103**, 9589 (1999).
[12] M. Prager and A. Heidemann, Chem. Rev. **97**, 2933 (1997).

[13] R. M. Dimeo and D. A. Neumann, Phys. Rev. B **63**, 014301 (2000).

[14] C. Gutt, B. Asmussen, I. Krasnov, W. Press, W. Langel, and R. Kahn, Phys. Rev. B **59**, 8607 (1999).

[15] M. Bienfait, B. Asmussen, P. Zeppenfeld *et al.*, Physica B **301**, 292 (2001).

[16] J. A. MacKinnon, J. Eckert, D. F. Coker, and A. L. R. Bug, J. Chem. Phys. **114**, 10137 (2001).

[17] H. van Koningsveld, F. Tuinstra, H. van Bekkum, and J. C. Jansen, Acta Crystallogr., Sect. B: Struct. Sci. **45**, 423 (1989).

[18] P. J. Breen, J. A. Warren, E. R. Bernstein, and J. I. Seeman, J. Am. Chem. Soc. **109**, 3453 (1987).

[19] U. Muller, A. Brenner, A. Reich, and K. K. Unger, ACS Symp. Ser. **398**, 346 (1989).

[20] Manufacturers are identified in order to provide complete identification of experimental conditions, and such identification is not intended as a recommendation or endorsement by NIST.

[21] See http://www.ncnr.nist.gov/dave/

[22] A. C. Larson and R. B. Von Dreele, Los Alamos National Laboratory Report No. LAUR 86-748, 2000 (unpublished).

[23] B. H. Toby, J. Appl. Crystallogr. **34**, 210 (2001).

[24] R. E. Dinnebier, Powder Diffr. **14**, 84 (1999).

[25] J. Colmenero, R. Mukhopadhyay, A. Alegria, and B. Frick, Phys. Rev. Lett. **80**, 2350 (1998).

[26] I. Jencic, J. Peternelj, B. Cvikl, and M. M. Pintar, Z. Phys. B: Condens. Matter **79**, 251 (1990).

[27] S. Clough, A. Heidemann, A. H. Horsewill, and M. N. J. Paley, Z. Phys. B: Condens. Matter **55**, 1 (1984).

[28] P. Schiebel, G. J. Kearley, and M. R. Johnson, J. Chem. Phys. **108**, 2375 (1998).

[29] P. Schiebel, A. Hoser, W. Prandl, G. Heger, W. Paulus, and P. Schweiss, J. Phys.: Condens. Matter **6**, 10989 (1994).

[30] W. Press, *Single Particle Rotations in Molecular Crystals* (Springer, Berlin, 1991), p. 61.

[31] W. Hausler and A. Huller, Z. Phys. B: Condens. Matter **59**, 177 (1985).

[32] D. W. Matuschek and A. Huller, Can. J. Chem. **66**, 495 (1988).

[33] A. J. Horsewill and Q. Xue, Phys. Chem. Chem. Phys. **4**, 5475 (2002).

[34] A. Detken, P. Schiebel, M. R. Johnson, H. Zimmermann, and U. Haeberlen, Chem. Phys. **238**, 301 (1998).

[35] S. Clough, A. Heidemann, A. J. Horsewill, J. D. Lewis, and M. N. J. Paley, J. Phys. C **15**, 2495 (1982).

[36] A. J. Horsewill, Progr. Nucl. Magn. Res. Spectrosc. **35**, 359 (1999).

[37] A. K. Rappe, C. J. Casewit, K. S. Colwell, W. A. Goddard III, and W. M. Skiff, J. Am. Chem. Soc. **114**, 10024 (1992).

[38] B. F. Mentzen and F. Bosselet, C. R. Acad. Sci. URSS **309**, 539 (1989).